Check for updates

ASME Letters in Dynamic Systems and Control
Online journal at:
https://asmedigitalcollection.asme.org/lettersdynsys

Hybrid Optimal Control of a Flying+Sailing Drone[1]

Taha Yasini[2]
Department of Mechanical Engineering,
University of Alabama,
Tuscaloosa, AL 35401
e-mail: tyasini@crimson.ua.edu

Ali Pakniyat
Assistant Professor
Department of Mechanical Engineering,
University of Alabama,
Tuscaloosa, AL 35401
e-mail: apakniyat@ua.edu

This paper studies the combined maneuver of flying and sailing for a robotic system which is referred to as a flying+sailing drone. Due to the emergence of hybrid systems behavior in tasks which involve both the flying and sailing modes, a hybrid systems formulation of the robotic system is presented. Key characteristics of the system are (i) changes in the dimension of the state space as the system switches from flying to sailing and vice versa and (ii) the presence of autonomous switchings triggered only upon the landing of the drone on the water surface. For the scenario in which the drone's initial state is given in the flying mode and a fixed terminal state is specified in the sailing mode, the associated optimal control problems are studied within the vertical plane passing through the given points, hence the dynamics of the drone in the flying mode are represented in a five-dimensional state space (associated with three degrees-of-freedom) and in a three-dimensional state space in the sailing mode (associated with two degrees-of-freedom). In particular, the optimal control problems for the minimization of time and the minimization of the control effort are formulated, the associated necessary optimality conditions are obtained from the hybrid minimum principle (HMP), and the associated numerical simulations are presented. [DOI: 10.1115/1.4063603]

Keywords: hybrid systems, nonlinear control, nonlinear systems, optimal controls, optimization algorithms, robotics, switched systems, vehicle dynamics and control

1 Introduction

Over the past few decades, the need for multi-modal autonomous robotics systems has emerged in several civil, commercial, and military applications. As remarked by Ref. [1], for quick and efficient military organizations, there is a grave need for a combined robotic system capable of providing services of energy-efficient but slow-moving ships combined with fast but energy-consuming planes. The emergence of these multi-modal control systems calls for the development of fast and efficient control synthesis algorithms capable of handling the "hybrid" nature of these systems. Moreover, fulfilling requirements such as the minimization of time and the minimization of energy consumption in performing the tasks is a significant aspect of the control synthesis in several applications, e.g., in the search and rescue of humans in coastal cities, where quick human detection is vital [2–4].

There is now an extensive literature on robotic systems capable only of either flying or sailing. A review of the developments on autonomous sailboats and their application is presented in Ref. [5]. The stochastic dynamic programming approach for time-optimal control of sailing drones is presented in Ref. [6]. The algorithm for path planning of minimum time problem is introduced in Ref. [7]. The path planning optimization problem of unmanned sailboats is investigated in Ref. [8]. The optimal control of flying drones has also been extensively studied in the literature, e.g., in Ref. [9], an algorithm for the minimum time of a quadrotor based on Pontryagin's minimum principle is presented; Ref. [10] studies the time-optimal control problem subject to changes in the environment and encounters with unknown disturbances; and Refs. [11–14] study the time-optimal control problems for drones in various situations.

This paper focuses on the presentation of a hybrid systems formulation for a drone capable of both flying and sailing and provides solutions to the associated hybrid optimal control problems for the minimization of time and the minimization of the control effort of tasks involving both the flying and sailing modes. The theoretical foundation of this work relies on the hybrid minimum principle (HMP) which has been extensively researched in the control theory literature [15–20]. The HMP has been implemented on several engineering systems and, in particular, on various automotive systems, see, e.g., Refs. [21–24].

Key aspects of hybrid systems exhibited by the flying+sailing drone are (i) the presence of both autonomous and control switchings, (ii) the presence of state jumps at switching instances, and (iii) changes in the dimension of the state space upon switching between different modes. Hence, we invoke the version of the HMP with explicit expressions of the boundary conditions for the Hamiltonians and adjoint processes as well as the associated HMP-based multiple autonomous switching (HMP–MAS) algorithm established in Ref. [20] in order to present a hybrid systems formulation of the multi-mode drone, to obtain the necessary optimality conditions, and to solve for the associated optimal inputs and trajectories.

The main contribution of this paper is that a new class of drones capable of both flying and sailing is modeled and optimally controlled within the hybrid systems framework which, to the best of

[1]Paper presented at the 2023 Modeling, Estimation, and Control Conference (MECC 2023), Lake Tahoe, NV, Oct. 2–5. Paper No. MECC2023-26.
[2]Corresponding author.
Manuscript received July 24, 2023; final manuscript received September 24, 2023; published online October 31, 2023. Assoc. Editor: Wen-Chiao Lin.

Copyright © 2023 by ASME

ed from http://asmedigitalcollection.asme.org/lettersdynsys/article-pdf/3/3/031008/7056347/aldsc_3_3_031008.pdf?casa_token=qd0HG9nAIHwAAAAA:SNvSK8K64KEZmP8Om87_mxkhfGGRNn2f5as9Z433Y_EY5DvxCzwbXnrjr2cUdoGylsdcKM by Colorado At Boulder user on 01 October 20

our knowledge, has not appeared before in the literature. In addition to flying+sailing drones, the theoretical foundations and numerical algorithms in this paper are applicable to a broad class of multimodal robotics systems.

The scenario studied in this article is the motion of the drone in a vertical plane passing through the initial position and a desired terminal position, where the initial condition is provided in the flying mode and the terminal conditions are in the sailing mode; hence, the drone must switch from the flying mode to the sailing mode at an intermediate time during its motion, where this switching in dynamics becomes possible only when the drone's location coincides with a locus on the loci of points on the water surface. Upon switching of the dynamics from flying to sailing, the dimension of the state space necessarily changes as the vertical motion of the drone becomes restricted to the water surface.

The structure of the paper is as follows. Section 2 presents hybrid systems formulation of the flying+sailing drone. Section 3 presents the HMP and the associated HMP–MAS algorithm. The implementation of the HMP for the minimization of the total control effort, and for the minimization of the time required for the drone to reach the desired terminal state from its initial state are, respectively, presented in Secs. 4 and 5. Numerical simulations are presented in Sec. 6. Conclusion and future research directions are presented in Sec. 7.

2 Hybrid Systems Model of the Drone

2.1 Problem Definition and Modeling Assumptions. We consider a drone capable of both flying and sailing. For the scenario shown in Fig. 1, the drone begins its maneuver in flying mode and aims to reach a fixed terminal state over the water surface. In this scenario, a segment of the trajectory corresponds to flying and the other segment corresponds to sailing, thus the system is exhibiting hybrid systems behavior. In the current study, we assume that the change of dynamics from flying to sailing and vice versa are instantaneous, i.e., the time and the associated control effort for transitioning between the two modes are negligible. This instantaneous change assumption, in particular, includes the immediate change in the pitch angle of the drone, as shown in Fig. 1, where the drone's configuration right after the switching (the initiation of the sailing mode) displayed in gray immediately follows the drone's configuration just before the switching (the termination of the flying mode) displayed in black. While this simplifying assumption introduces errors in the dynamics modeling and costs, these errors are within a tolerable range in a simplified model of the robotic system considered in this paper; a more detailed modeling and controller synthesis with the consideration of the transition phase as a separate mode in the hybrid systems formulation of the system is a part of future investigations.

A key characteristic of hybrid systems exhibited by this robotic system is the change in the dimension of the state space as the system switches from flying to sailing and vice versa. Another key characteristic of hybrid systems in this system is the presence of autonomous switching for the change of the dynamics from flying to sailing, which are triggered only when the drone reaches the water surface.

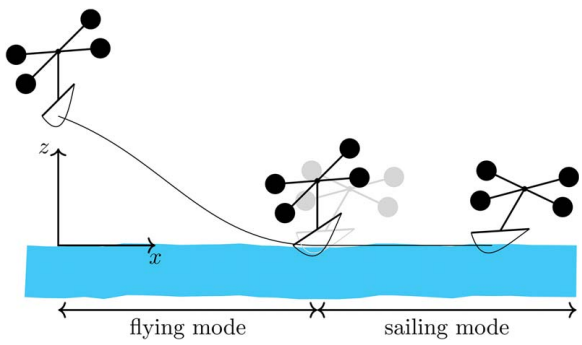

Fig. 1 Schematic view of the flying+sailing drone

2.2 Hybrid Problem Formulation. For scenarios where the maneuver occurs within the XZ plane passing through the initial and terminal positions and the yaw angle is within the same plane, the equation of motion of the drone can be simplified as an in-plane motion. For brevity of notation, we assume $m = g = 1$. The nondimensionalization state space dynamic of the drone in the flying mode is expressed as [9]

$$\dot{x}_{q_1} = \begin{bmatrix} \dot{x}_1 \\ \dot{x}_2 \\ \dot{x}_3 \\ \dot{x}_4 \\ \dot{x}_5 \end{bmatrix} = f_{q_1}(x_{q_1}, u) = \begin{bmatrix} x_2 \\ u_T \sin x_5 \\ x_4 \\ u_T \cos x_5 - 1 \\ u_R \end{bmatrix}, \quad t \in [0, t_s] \tag{1}$$

subject to the initial condition $x_{q_1}(t_0) = x_0$, where x_1 and x_3 are, respectively, the horizontal and vertical positions of the drone, x_2 and x_4 are, respectively, the horizontal and vertical velocities, and x_5 is the pitch angle, u_T is the thrust force, and u_R is the pitch rate, which are taking values from the set $[-2, +2]$. The dynamics of the drone in the sailing mode are written as

$$\dot{x}_{q_2} = \begin{bmatrix} \dot{x}_1 \\ \dot{x}_2 \\ \dot{x}_3 \end{bmatrix} = f_{q_2}(x_{q_2}, u) = \begin{bmatrix} x_2 \\ u_T \sin x_3 \\ u_R \end{bmatrix}, \quad t \in [t_s, t_f] \tag{2}$$

where x_1, x_2, u_T, and u_R are as before, and x_3 is the pitch angle. At the switching instant, the system's state before and after switching are related by the boundary condition

$$x_{q_2}(t_s) = \xi_{q_1 q_2}(x_{q_1}(t_s -)) \equiv \xi_{q_1 q_2}\left(\lim_{t \to t_s} x_{q_1}(t)\right) \tag{3}$$

where t_s indicates the time of the autonomous switching of when the drone finishes flying and begins sailing, and $\xi_{q_1 q_2}$ is the state transition jump map described by

$$x_{q_2} = \xi_{q_1 q_2}(x_{q_1}) = \begin{bmatrix} x_1 \\ x_2 \\ x_5 + \delta \end{bmatrix} \tag{4}$$

where δ is the difference between the pitch angles in the flying and sailing modes. The switching manifold which is the condition required to be satisfied for the flying mode to end and for the sailing mode to begin and corresponds to the drone landing over the water surface is expressed by $m_{q_1 q_2}(x_{q_1}) = 0$, where

$$m_{q_1 q_2}(x_{q_1}) = x_3 \equiv z \tag{5}$$

The objective of the associated hybrid optimal control problem (HOCP) is to identify the inputs to minimize the hybrid performance expressed by

$$J = \int_0^{t_s} \ell_{q_1}\left(x_{q_1}(s), u(s)\right) \mathrm{d}s + \int_{t_s}^{t_f} \ell_{q_2}\left(x_{q_2}(s), u(s)\right) \mathrm{d}s \tag{6}$$

where ℓ_{q_1} and ℓ_{q_2} are cost functions associated with flying and sailing, respectively. In the problem of time minimization, the costs ℓ_{q_1}, ℓ_{q_2} are set to be equal to 1, and in the case of minimizing the control effort, these running cost functions are taken to be $\frac{1}{2} u^\top R u$, where $R = R^\top > 0$.

3 The Hybrid Minimum Principle and the Associated Algorithm

THEOREM 1 ([25, Theorem 3.2]). Consider the hybrid system $\mathbb{H}$ subjected to assumptions A0–A3 in [19, Appendix A] and the

Downloaded from http://asmedigitalcollection.asme.org/lettersdynsys/article-pdf/3/3/031008/7056347/aldsc_3_3_031008.pdf?casa_token=qd0HG9nAIHwAAAAA:SNvSK8K64kEZmP8Om87_mxkhfGGRNn2f5As9Z433Y_EY5DvxCzwbXnrjr2cUdoGylsdcKM by Colorado At Boulder user on 01 October 20

HOCP with the hybrid performance function (6). Define the family of system Hamiltonians as

$$H_q(x_q, \lambda_q, u_q, t) = \ell_q(x_q, u_q, t) + \lambda_q^\top f_q(x_q, u_q, t) \tag{7}$$

where in the current paper $q \in \{q_1, q_2\} \equiv \{flying, sailing\}$, $x_{flying}, \lambda_{flying} \in \mathbb{R}^5$, $x_{sailing}, \lambda_{sailing} \in \mathbb{R}^3$, and also u_{flying}, $u_{sailing} \in U \subset \mathbb{R}^2$. Then, for an optimal input u^* and along the corresponding optimal trajectory x^*, there exists an adjoint process λ^* such that

$$H_q\left(x_q^*, \lambda_q^*, u_q^*, t\right) \le H_q\left(x_q^*, \lambda_q^*, u_q, t\right) \tag{8}$$

where x_q^* and λ^* satisfy Hamiltonian canonical equations

$$\begin{aligned} \dot{x}_q^* &= \frac{\partial H_q}{\partial \lambda_q}(x_q^*, \lambda_q^*, u_q^*, t) \equiv f\left(x_q^*, u_q^*, t\right) \\ \dot{\lambda}_q^* &= -\frac{\partial H_q}{\partial x_q}(x_q^*, \lambda_q^*, u_q^*, t) \end{aligned} \tag{9}$$

$$\equiv -\frac{\partial \ell_q}{\partial x}\left(x_q^*, u_q^*, t\right) - \frac{\partial f_q}{\partial x}\left(x_q^*, u_q^*, t\right)^\top \lambda_q^* \tag{10}$$

subjected to

$$x_{q_1}^*(t_0) = x_0 \tag{11}$$

$$x_{q_2}^*(t_s) = \xi_{q_1 q_2}\left(x_{q_1}^*(t_s-)\right) \tag{12}$$

$$\lambda_{q_1}^*(t_s) = \nabla \xi_{q_1 q_2}\big|^\top_{x_{q_1}(t_s-)} \lambda_{q_2}^*(t_s+) + p \nabla m|_{x_{q_1}(t_s-)} \tag{13}$$

$$x_{q_2}^*(t_f) = x_f \tag{14}$$

Moreover, at the optimal switching time t_s, the Hamiltonian satisfies

$$H_{q_1}(x^*, \lambda^*, u^*)\big|_{t_s-} = H_{q_2}(x^*, \lambda^*, u^*)\big|_{t_s+} \tag{15}$$

In addition, whenever t_f is not a priori fixed (in the time-optimal case), the Hamiltonian satisfies

$$H_{q_2}(x^*, \lambda^*, u^*)|_{t_f} = 0 \tag{16}$$

The associated HMP–MAS algorithm [20] for the flying+sailing drone is presented in Algorithm 1.

Algorithm 1 HMP–MAS algorithm for the flying+sailing drone

System Initialization
while $\mu > \varepsilon_f$ **do**
  For each mode q, solve TP-BVP using Eqs. (9) and (10)
  Calculate p using Eq. (19)
  Update t_s using Eq. (17)
  Update y_s using Eq. (18)
  Update μ using Eq. (20)
end while

At the beginning step of the HMP–MAS algorithm for flying +sailing drone, initial values including termination tolerance ε_f, step size r_k, are fixed, the iteration counter is set to zero, i.e., $k = 0$, switching time t_s^k and the pre-switching state $y_s^k = x_{q_1}(t_s-) \equiv x_{q_1}(t_s)$ are initiated.

In each iteration, two sets of decoupled two-point boundary value problems (TP-BVP) are solved, and then the corresponding couplings appear in the updates, which yield new switching pairs t_s^{k+1} and y_s^{k+1} as

$$\begin{aligned} t_s^{k+1} &= t_s^k - r_k\left(H_{q_1}^k - H_{q_2}^k\right) \\ y_s^{k+1}(t_s) &= y_s^k(t_s) - r_k m^k(t_s) \nabla m \end{aligned} \tag{17}$$

$$-r_k\left(\nabla \xi_{q_1 q_2}^\top \lambda_{q_2}^k(t_s) + p^k \nabla m - \lambda_{q_1}^k(t_s)\right) \tag{18}$$

where the scalar p is

$$p^k = \frac{H_{q_2}^k - H_{q_1}^k + f_{q_1}^k(t_s)^\top\left(\lambda_{q_1}^k(t_s) - \nabla \xi_{q_1 q_2}^\top \lambda_{q_2}^k(t_s)\right)}{\left(f_{q_1}^k(t_s)\right)^\top \nabla m_i^k} \tag{19}$$

As established in Ref. [20], the updates (17) and (18) result in convergence to the optimal switching time t_s and optimal switching point y_s and these updates correspond to decent directions of the auxiliary cost

$$\mu_k = \left\| \begin{bmatrix} H_{q_1}^k - H_{q_2}^k \\ \nabla \xi_{q_1 q_2}^\top \lambda_{q_2}^k(t_s) + p^k \nabla m - \lambda_{q_1}^k(t_s) \end{bmatrix} \right\|^2 + \left|m^k(t_s)\right|^2 \tag{20}$$

4 The Minimum Control Effort Problem

In this section, the HMP is presented for the flying+sailing drone in order to calculate control effort minimization. The corresponding steps in the HMP are as follows:

4.1 Hamiltonian Minimization. The Hamiltonian for flying mode is written as

$$\begin{aligned} H_{q_1} = \ell_{q_1} + \lambda_{q_1}^\top f_{q_1} = \frac{1}{2} u^\top R u + \lambda_1 x_2 + \lambda_2 u_T \sin x_5 \\ + \lambda_3 x_4 + \lambda_4 (u_T \cos x_5 - 1) + \lambda_5 u_R \end{aligned} \tag{21}$$

and the Hamiltonian for sailing mode is expressed as

$$H_{q_2} = \ell_{q_2} + \lambda_{q_2}^\top f_{q_2} = \frac{1}{2} u^\top R u + \lambda_1 x_2 + \lambda_2 u_T \sin x_3 + \lambda_3 u_R \tag{22}$$

Thus the Hamiltonian minimization for flying mode yields

$$\frac{\partial H_{q_1}}{\partial u} = 0 \Rightarrow \begin{bmatrix} u_T \\ u_R \end{bmatrix} = -\begin{bmatrix} \lambda_2 \sin x_5 + \lambda_4 \cos x_5 \\ \lambda_5 \end{bmatrix} \tag{23}$$

and for sailing mode, it yields

$$\frac{\partial H_{q_2}}{\partial u} = 0 \Rightarrow \begin{bmatrix} u_T \\ u_R \end{bmatrix} = -\begin{bmatrix} \lambda_2 \sin x_3 \\ \lambda_3 \end{bmatrix} \tag{24}$$

4.2 Continuous State Evolution. The continuous state dynamics from the Hamiltonian canonical Eq. (9) are equal to the dynamics of flying and sailing modes (1) and (2) with the substitution of Eqs. (23) and (24) for the inputs, subject to the initial, boundary, and terminal conditions

$$x_{q_1}(t_0) = x_0 \tag{25}$$

$$x_{q_2}(t_s) = \xi_{q_1 q_2}\left(x_{q_1}(t_s)\right) \tag{26}$$

$$x_{q_2}(t_f) = \begin{bmatrix} x(t_f) \\ \dot{x}(t_f) \\ \theta(t_f) \end{bmatrix} \tag{27}$$

where the autonomous transition dynamic from the flying mode to the sailing mode is subject to the switching manifold condition

$$m_{q_1 q_2}(x_{q_1}) \equiv z = 0 \tag{28}$$

Downloaded from http://asmedigitalcollection.asme.org/lettersdynsys/article-pdf/3/3/031008/7056347/aldsc_3_3_031008.pdf?casa_token=qd0HG9nAIHwAAAAA:SNvSK8K64kEZmP8Om87_mxkhfGGRNn2f5As92433Y_EY5DvxCzwbXnrjr2cUdoGylsdcKM by Colorado At Boulder user on 01 October 20

4.3 Evolution of the Adjoint Process. The Hamiltonian canonical Eq. (10) in the HMP yields the dynamics of the adjoint process for flying mode in $t \in [0, t_s]$ as

$$\dot{\boldsymbol{\lambda}}_{q_1} = -\frac{\partial H_{q_1}}{\partial \mathbf{x}_{q_1}} = \begin{bmatrix} \dot{\lambda}_1 \\ \dot{\lambda}_2 \\ \dot{\lambda}_3 \\ \dot{\lambda}_4 \\ \dot{\lambda}_5 \end{bmatrix} = \begin{bmatrix} 0 \\ -\lambda_1 \\ 0 \\ -\lambda_3 \\ \lambda_4 u_T \sin x_5 - \lambda_2 u_T \cos x_5 \end{bmatrix} \tag{29}$$

which, with the substitution of Eq. (23), $\dot{\lambda}_5$ is expressed as

$$\dot{\lambda}_5 = \left(\lambda_2^2 - \lambda_4^2\right) \sin x_5 \cos x_5 - \lambda_4 \lambda_2 \left(\sin^2 x_5 - \cos^2 x_5\right) \tag{30}$$

Furthermore, the dynamics of the adjoint process for sailing mode in $t \in [t_s, t_f]$ is written as

$$\dot{\boldsymbol{\lambda}}_{q_2} = -\frac{\partial H_{q_2}}{\partial \mathbf{x}_{q_2}} = \begin{bmatrix} \dot{\lambda}_1 \\ \dot{\lambda}_2 \\ \dot{\lambda}_3 \end{bmatrix} = \begin{bmatrix} 0 \\ -\lambda_1 \\ -\lambda_2 u_T \cos x_3 \end{bmatrix} \tag{31}$$

where with the substitution of Eq. (24), $\dot{\lambda}_3$ is written as

$$\dot{\lambda}_3 = \lambda_2^2 \sin x_3 \cos x_3 \tag{32}$$

The boundary conditions for λ are determined from

$$\boldsymbol{\lambda}_{q_1}(t_s) = \nabla \xi_{q_1 q_2}\big|^{\top}_{x_{q_1}(t_s-)} \boldsymbol{\lambda}_{q_2}(t_s+) + p \nabla m|_{x_{q_1}(t_s-)} \tag{33}$$

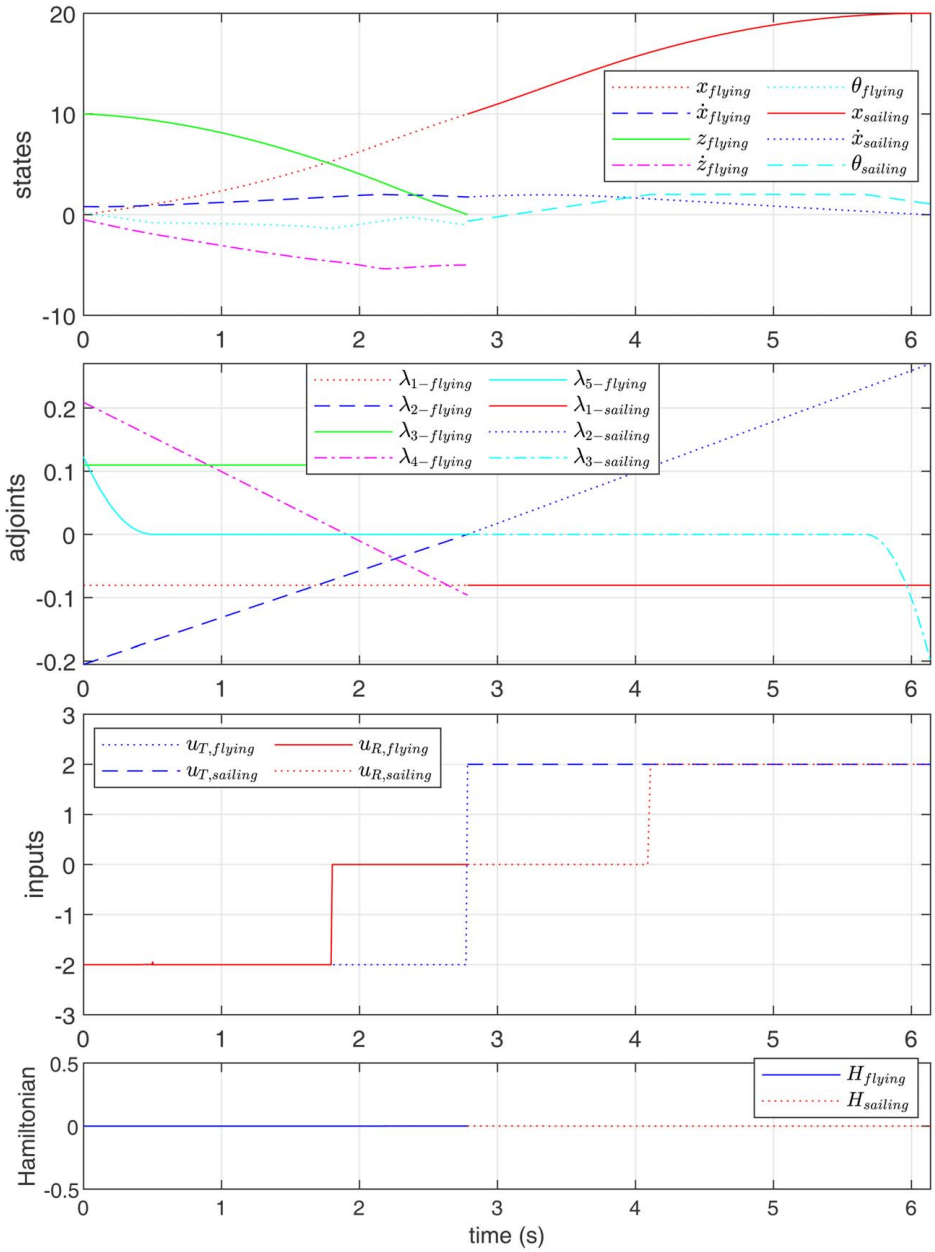

Fig. 2 The flying+sailing drone states, the adjoint processes, control inputs, and the corresponding Hamiltonian for the minimum time problem

wnloaded from http://asmedigitalcollection.asme.org/lettersdynsys/article-pdf/3/3/031008/7056347/aldsc_3_3_031008.pdf?casa_token=qd0HG9nAIHwAAAAA:SNvSK8K64KEZmP8Om87_mxkhfGGRNn2f5As9Z433Y_EY5DvxCzwbXnrjr2cUdoGylsdcKM by Colorado At Boulder user on 01 October 20

5 The Minimum Time Problem

For establishing the results of the HMP for the minimization of the time, the corresponding steps are as follows.

5.1 Flying Mode. The Hamiltonian for flying mode is written as

$$H_{q_1} = \ell_{q_1} + \lambda_{q_1}^{\top} f_{q_1} = 1 + \lambda_1 x_2 + \lambda_2 u_T \sin x_5 + \lambda_3 x_4 + \lambda_4 (u_T \cos x_5 - 1) + \lambda_5 u_R \tag{34}$$

The Hamiltonian minimization (8) for the Hamiltonian (34) yields the optimal values u_R^* and u_T^*, where for the input u_R we obtain

$$u_R^* = \underset{u_R \in [-2,\,+2]}{\operatorname{argmin}} \{\lambda_5 u_R\} \tag{35}$$

which takes the values -2 and $+2$ whenever λ_5 is, respectively, strictly positive and strictly negative. In order to determine the singular arcs corresponding to $\lambda_5 = 0$, we need to study the case of $\dot{\lambda}_5 = 0$ from Eq. (29), which yields

$$x_5^* = \arctan\left(\frac{\lambda_2}{\lambda_4}\right) \tag{36}$$

thus giving $u_{R,s}^*$ for singular arcs as

$$u_{R,s}^* = \dot{x}_5^* = \frac{\lambda_2 \lambda_3 - \lambda_1 \lambda_4}{\lambda_2^2 + \lambda_4^2} \tag{37}$$

Hence, the control input u_R^* for time-optimal is given by

$$u_R^* = \begin{cases} +2 & \text{if } \lambda_5 < 0 \\ u_{R,s}^* & \text{if } \lambda_5 = 0 \\ -2 & \text{if } \lambda_5 > 0 \end{cases} \tag{38}$$

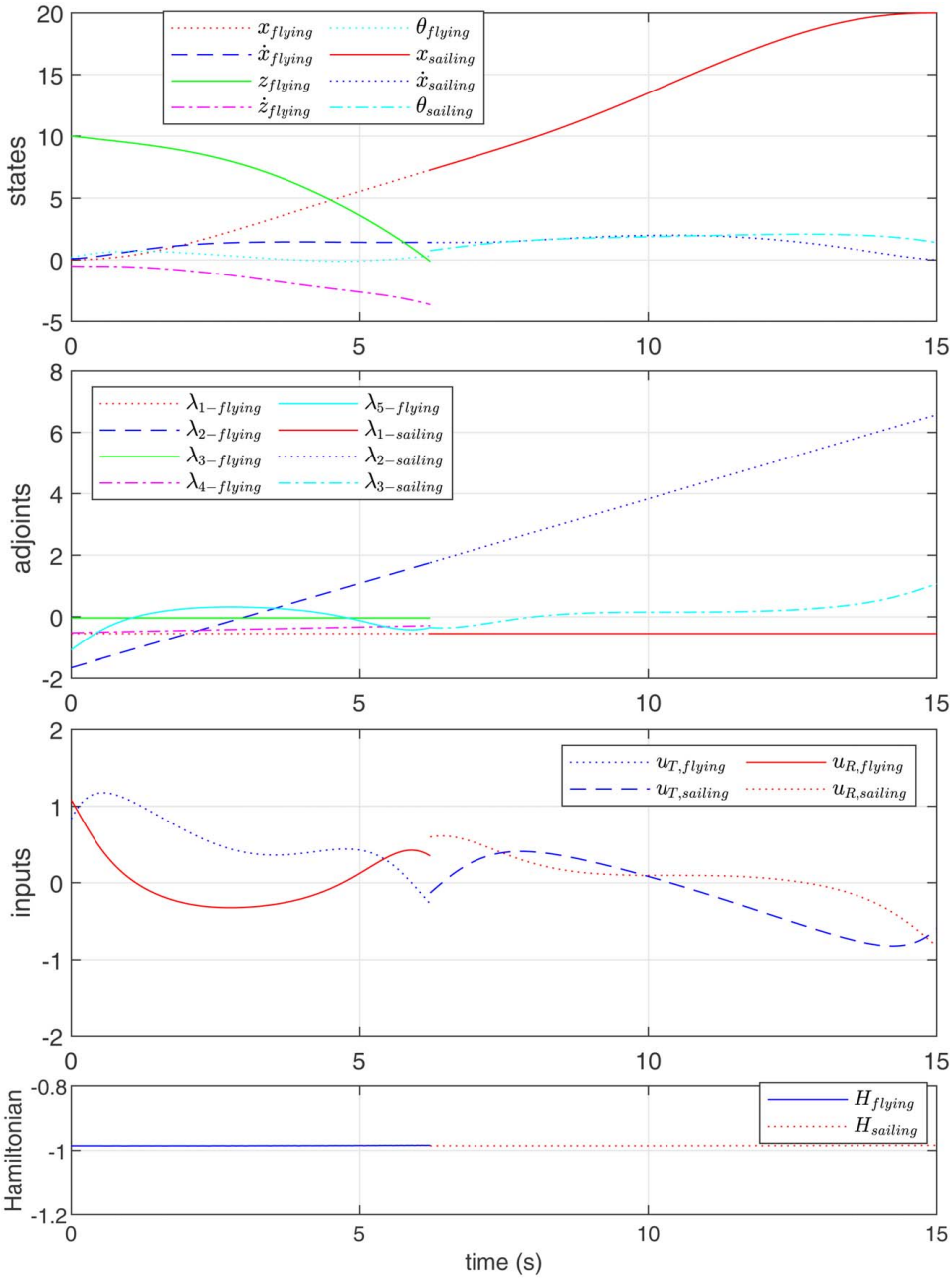

Fig. 3 The flying+sailing drone states, the adjoint processes, control inputs, and the corresponding Hamiltonian for the minimum control effort problem

Downloaded from http://asmedigitalcollection.asme.org/lettersdynsys/article-pdf/3/3/031008/7056347/aldsc_3_3_031008.pdf?casa_token=qd0HG9nAIHwAAAAA:SNvSK8K64KEZmP8Om87_mxkhfGGRNn2f5As9Z433Y_EY5DvxCzwbXnrjr2cUdoGylsdcKM by Colorado At Boulder user on 01 October 2023

Moreover, the control input u_T is obtained as

$$u_T^* = \underset{u_T \in [-2,\,+2]}{\operatorname{argmin}} \{\lambda_2 u_T \sin x_5 + \lambda_4 u_T \cos x_5\} \tag{39}$$

where the minimizing values of u_T, which depend on the sign of $(\lambda_2 \sin x_5 + \lambda_4 \cos x_5)$ are determined by

$$u_T^* = \begin{cases} +2 & \text{if } \lambda_2 \sin x_5 + \lambda_4 \cos x_5 \le 0 \\ -2 & \text{if } \lambda_2 \sin x_5 + \lambda_4 \cos x_5 > 0 \end{cases} \tag{40}$$

It is worth mentioning that the control input u_T^* does not contain singular arcs, see, e.g., Ref. [9].

5.2 Sailing Mode. The Hamiltonian for sailing mode is written as

$$H_{q_2} = \ell_{q_2} + \lambda_{q_2}^{\top} f_{q_2} = 1 + \lambda_1 x_2 + \lambda_2 u_T \sin x_3 + \lambda_3 u_R \tag{41}$$

Similar to Sec. 5.1 for control input u_R we obtain

$$u_R^* = \underset{u_R \in [-2,\,+2]}{\operatorname{argmin}} \{\lambda_3 u_R\} \tag{42}$$

Hence, control input u_R^* for sailing mode is expressed as

$$u_R^* = \begin{cases} +2 & \text{if } \lambda_3 < 0 \\ 0 & \text{if } \lambda_3 = 0 \\ -2 & \text{if } \lambda_3 > 0 \end{cases} \tag{43}$$

In addition, the control input u_T is obtained as

$$u_T^* = \underset{u_T \in [-2,\,+2]}{\operatorname{argmin}} \{\lambda_2 u_T \sin x_3\} \tag{44}$$

Hence, the optimal input u_T^* for sailing mode is given by

$$u_T^* = \begin{cases} +2 & \text{if } \lambda_2 \sin x_3 \le 0 \\ -2 & \text{if } \lambda_2 \sin x_5 > 0 \end{cases} \tag{45}$$

6 Numerical Simulation

We consider the initial condition of the drone to be in the flying mode with $x_{q_1}(t_0 = 0) = [0,\, 0.1,\, 10,\, -0.5,\, \pi/16]^{\top}$ and study the case where the drone aims to reach a fixed terminal location with $x(t_f) = 20$ m over the surface of the water, i.e., $z(t_f) = 0$. We consider $\delta = 25$ deg for the instantaneous change in the pitch angle at the switching instance. The results for the time-optimal problem including states, adjoints, control inputs, and Hamiltonian are shown in Fig. 2. The optimal inputs u_T and u_R obtained from Eqs. (38), (40), (43), and (45) for the time-optimal problem are displayed in Fig. 2 which, due to the bang-bang nature of minimum time solutions, these values switch between −2 and +2. The minimum terminal time is obtained as $t_f = 6.138$ s and the optimal switching time is $t_s = 2.783$ s. In this solution, the optimal states at the switching instant are $x_{q_1}(t_s) = [9.51,\, 1.78,\, 0,\, -3.17,\, -1.05]^{\top}$.

The results of the optimal control problem including states, adjoints, control inputs, and Hamiltonian for the minimization of control effort over a period of $[t_0,\, t_f] = [0,\, 15]$ with a fixed terminal state are shown in Fig. 3. In this scenario, the optimal autonomous switching between flying and sailing modes occurs at $t_s = 6.2$ s at the optimal switching state $x_{q_1}(t_s) = [7.26,\, 1.42,\, 0,\, -3.64,\, -0.31]^{\top}$.

Fig. 4 The flying+sailing drone Splash Drone 4 by Swellpro

7 Concluding Remarks

This paper presents a hybrid systems formulation for a robotic system with maneuvers consisting of both flying and sailing. The presented hybrid systems formulation captures the key aspects of these robotic systems and, in particular, the changes in the dimension of the state space as the system switches from flying to sailing and vice versa, as well as the presence of autonomous switching which is triggered only upon the landing of the drone over the water surface. In this study, the transition time between flying and sailing is considered to be negligible, hence the hybrid systems model does not include a separate mode for the intermediate phase in which the drone has landed on the water but is not yet fully operating in the lower dimensional sailing mode. This simplifying assumption is justified considering that at this stage, only a high-level control synthesis is being studied. The necessary optimality conditions of the HMP and the associated HMP–MAS algorithm for numerical simulations are shown to be effective tools in providing solutions to the associated hybrid optimal control problems both for the minimization of time and the minimization of the control effort for the multi-modal robotic system. It shall be remarked, however, that due to the nonlinear nature of the drone dynamics, numerical solutions of the associated TP-BVPs are sensitive to the initial guess, especially for the state component $x_5 \equiv \theta$. Moreover, the HMP–MAS algorithm for the determination of optimal time switching t_s and optimal switching states is slowly converging (an order of 10^5 iterations is required for convergence) and, hence, recalculations are time-consuming.

Future research directions include establishing a more detailed dynamics model considering all six degrees-of-freedom in the flying mode and five degrees-of-freedom in the sailing mode, and solving the associated hybrid optimal control problems employing the HMP–MAS algorithm. Another future direction is the accommodation of obstacle avoidance in the controller synthesis. A third line of future work includes the implementation of these theoretical results on an actual flying+sailing drone, particularly on Splash Drone 4 by Swellpro displayed in Fig. 4 as well as testing the multi-modal robotic system in real environments. An essential step in the practical implementation of the results, as mentioned earlier, is to establish separate hybrid modes for the transitioning of the drone from flying to sailing and vice versa based on the dynamics behavior of the corresponding robotic system.

Conflict of Interest

There are no conflicts of interest.

Data Availability Statement

The authors attest that all data for this study are included in the paper.

References

[1] Ackerman, E., 2022, "Darpa Reincarnates Soviet-Era Sea Monster: Concept Sea Skimmer to Fly Meters Above the Ocean," IEEE Spect., **59**(9), pp. 6–13.

[2] Qingqing, L., Taipalmaa, J., Queralta, J. P., Gia, T. N., Gabbouj, M., Tenhunen, H., Raitoharju, J., and Westerlund, T., 2020, "Towards Active Vision With

Downloaded from http://asmedigitalcollection.asme.org/lettersdynsys/article-pdf/3/3/031008/7056347/aldsc_3_3_031008.pdf?casa_token=qd0HG9nAIHwAAAAA:SNvSK8K64KEZmP8Om87_mxkhfGGRNn2f5as9Z433Y_EY5DvxCzwbXnrj2cUdoGylsdcKM by Colorado At Boulder user on 01 October 20

UAVS in Marine Search and Rescue: Analyzing Human Detection at Variable Altitudes," 2020 IEEE International Symposium on Safety, Security, and Rescue Robotics, Abu Dhabi, UAE, Nov. 4–6, pp. 65–70.
[3] Zwick, M., Gerdts, M., and Stütz, P., 2023, "Sensor-Model-Based Trajectory Optimization for UAVS to Enhance Detection Performance: An Optimal Control Approach and Experimental Results," Sensors, **23**(2), p. 664.
[4] Ho, W.-C., Shen, J.-H., Liu, C.-P., and Chen, Y.-W., 2022, "Research on Optimal Model of Maritime Search and Rescue Route for Rescue of Multiple Distress Targets," J. Marine Sci. Eng., **10**(4), p. 460.
[5] An, Y., Yu, J., and Zhang, J., 2021, "Autonomous Sailboat Design: A Review From the Performance Perspective," Ocean Eng., **238**, p. 109753.
[6] Shepherd, B., Haydon, B., and Vermillion, C., 2020, "Serious Sailing: Time-Optimal Control of Sailing Drones in Stochastic, Spatiotemporally Varying Wind Fields," 2020 American Control Conference (ACC), Denver, CO, July 1–3, pp. 5125–5130.
[7] Sidoti, D., Pattipati, K. R., and Bar-Shalom, Y., 2023, "Minimum Time Sailing Boat Path Algorithm," IEEE J. Ocean. Eng., **48**, pp. 307–322.
[8] Shen, Z., Ding, W., Liu, Y., and Yu, H., 2023, "Path Planning Optimization for Unmanned Sailboat in Complex Marine Environment," Ocean Eng., **269**, p. 113475.
[9] Hehn, M., Ritz, R., and D'Andrea, R., 2012, "Performance Benchmarking of Quadrotor Systems Using Time-Optimal Control," Auton. Rob., **33**, pp. 69–88.
[10] Romero, A., Penicka, R., and Scaramuzza, D., 2022, "Time-Optimal Online Replanning for Agile Quadrotor Flight," IEEE Rob. Autom. Lett., **7**(3), pp. 7730–7737.
[11] Foehn, P., Romero, A., and Scaramuzza, D., 2021, "Time-Optimal Planning for Quadrotor Waypoint Flight," Sci. Rob., **6**(56), p. eabh1221.
[12] Ryou, G., Tal, E., and Karaman, S., 2021, "Multi-fidelity Black-Box Optimization for Time-Optimal Quadrotor Maneuvers," Int. J. Rob. Res., **40**(12–14), pp. 1352–1369.
[13] Spedicato, S., and Notarstefano, G., 2017, "Minimum-Time Trajectory Generation for Quadrotors in Constrained Environments," IEEE Trans. Control Syst. Technol., **26**(4), pp. 1335–1344.
[14] Penin, B., Spica, R., Giordano, P. R., and Chaumette, F., 2017, "Vision-Based Minimum-Time Trajectory Generation for a Quadrotor UAV," 2017 IEEE/RSJ International Conference on Intelligent Robots and Systems (IROS), Vancouver, BC, Canada, Sept. 24–28, IEEE, pp. 6199–6206.
[15] Riedinger, P., lung, C., and Kratz, F., 2003, "An Optimal Control Approach for Hybrid Systems," Eur. J. Control, **9**(5), pp. 449–458.
[16] Garavello, M., and Piccoli, B., 2005, "Hybrid Necessary Principle," SIAM J. Control Optim., **43**(5), pp. 1867–1887.
[17] Shaikh, M. S., and Caines, P. E., 2007, "On the Hybrid Optimal Control Problem: Theory and Algorithms," IEEE Trans. Automat. Contr., **52**(9), pp. 1587–1603.
[18] Pakniyat, A., and Caines, P. E., 2016, "On the Stochastic Minimum Principle for Hybrid Systems," 2016 IEEE 55th Conference on Decision and Control (CDC), Las Vegas, NV, Dec. 12–14, IEEE, pp. 1139–1144.
[19] Pakniyat, A., and Caines, P. E., 2017, "Hybrid Optimal Control of an Electric Vehicle With a Dual-Planetary Transmission," Nonlinear Anal. Hybrid Syst., **25**, pp. 263–282.
[20] Pakniyat, A., and Caines, P. E., 2021, "On the Hybrid Minimum Principle: The Hamiltonian and Adjoint Boundary Conditions," IEEE Trans. Automat. Contr., **66**(3), pp. 1246–1253.
[21] Rahimi Mousavi, M. S., Pakniyat, A., Wang, T., and Boulet, B., 2015, "Seamless Dual Brake Transmission for Electric Vehicles: Design, Control and Experiment," Mech. Mach. Theory, **94**, pp. 96–118.
[22] Boulet, B., Mousavi, M. S. R., Alizadeh, H. V., and Pakniyat, A., 2017, "Seamless Transmission Systems and Methods for Electric Vehicles," July 11, US Patent 9702438.
[23] Kim, N., Cha, S., and Peng, H., 2010, "Optimal Control of Hybrid Electric Vehicles Based on Pontryagin's Minimum Principle," IEEE Trans. Control Syst. Technol., **19**(5), pp. 1279–1287.
[24] Xie, S., Hu, X., Xin, Z., and Brighton, J., 2019, "Pontryagin's Minimum Principle Based Model Predictive Control of Energy Management for a Plug-In Hybrid Electric Bus," Appl. Energy, **236**, pp. 893–905.
[25] Pakniyat, A., 2016, "Optimal Control of Deterministic and Stochastic Hybrid Systems: Theory and Applications", Ph.D. thesis, Department of Electrical & Computer Engineering, McGill University, Montreal, Canada.

wnloaded from http://asmedigitalcollection.asme.org/lettersdynsys/article-pdf/3/3/031008/7056347/aldsc_3_3_031008.pdf?casa_token=qd0HG9nAIHwAAAAA:SNvSK8K64KEZmP8Om87_mxkhfGGRNn2f5As9Z433Y_EY5DvxCzwbXnrjr2cUdoGylsdcKM by Colorado At Boulder user on 01 October 20